IEEE Access
Multidisciplinary | Rapid Review | Open Access Journal

Received June 24, 2019, accepted June 25, 2019, date of publication June 28, 2019, date of current version July 16, 2019.

Digital Object Identifier 10.1109/ACCESS.2019.2925714

Nonlinear Multi-Body Dynamic Modeling and Coordinated Motion Control Simulation of Deep-Sea Mining System

YU DAI[1,2], WANWU YIN[1], AND FEIYUE MA[1]
[1]College of Mechanical and Electrical Engineering, Central South University, Changsha 410083, China
[2]State Key Laboratory of Ocean Engineering, Shanghai Jiao Tong University, Shanghai 200240, China

Corresponding author: Yu Dai (daiyu_6@aliyun.com)

This work was supported in part by the National Natural Science Foundation of China under Grant 51774324, and in part by the National Key Research and Development Program of China under Grant SQ2016YF010109.

ABSTRACT In this paper, a nonlinear integrated multi-body dynamic (MBD) model of a deep-sea mining (DSM) system was developed. A particular nonlinear interaction model between the mining vehicle and the seabed sediment was derived. The fluid resistance and the resistance torque acting on the vehicle were obtained by the computational fluid dynamics (CFD) numerical simulations. In addition, a rigid-flexible coupled discrete element method (DEM) was adopted to model an extremely long mining riser efficiently and accurately. Developed by the C# program, a user-defined subprogram was intended to establish the DEM model of the riser. A motion control system model for trajectory tracking of the vehicle was developed in which the fuzzy control algorithm and the fuzzy adaptive PID control algorithm were used to control the speed and speed ratio of the tracks, respectively. Furthermore, the collaborative simulation between the dynamic model and the control model was achieved, and a coordinated motion mode for the total mining system was proposed and simulated. Accordingly, the trajectory tracking accuracy and slip of the vehicle, the spatial state change of the riser, and the interaction forces among subsystems were analyzed. This paper can provide a valuable theoretical basis and technical reference for the integrated design, performance prediction, and operation control of the practical DSM system.

INDEX TERMS Deep-sea mining system, nonlinear multi-body dynamic model, trajectory tracking control, collaborative simulation, coordinated motion.

I. INTRODUCTION

With the gradual depletion of land resources available, the exploitation and use of seafloor poly-metallic mineral resources are grabbing more attention from the international community, especially the global mining industry, and commercial exploitation is expected to start in the near future. A promising and continuous DSM system has been proposed and demonstrated in Fig. 1, including a seabed mining vehicle, flexible and rigid risers, a buffer, a submerged lift pump, and a mining vessel [1].

To evaluate the dynamics and trafficability of seabed mining vehicles, Dai *et al.* [2]–[4] have established series of MBD models for various vehicles to mine different seabed mineral resources, such as seabed nodule mining vehicles and poly-metallic sulfide mining vehicles, and simulations for the climbing, obstacle-crossing, ditch-crossing were performed and evaluated. Li and Zhong [5] established a prototype of a seabed mining vehicle and evaluated its trafficability through dynamic simulations. A formula was derived by Xu *et al.* [6] for calculating the turning traction force in consideration of the pushing resistance and sinkage of the vehicle, and the effects of the turning speed, track pitch and contacting length on the turning traction force were investigated. Umaru *et al.* [7] developed equations and models for tracked vehicles during steering motions, and pointed out that only the hydrodynamic force and traction force would be affected by the driving speed. Vu *et al.* [8] investigated the operations of a ladder trencher, analyzed its detailed mechanics affected by the ladder force and torque. Baek *et al.* [9] studied the soil thrust of an underwater vehicle and developed a prediction model of such. Additionally, a host of dynamic

The associate editor coordinating the review of this manuscript and approving it for publication was Jianyong Yao.

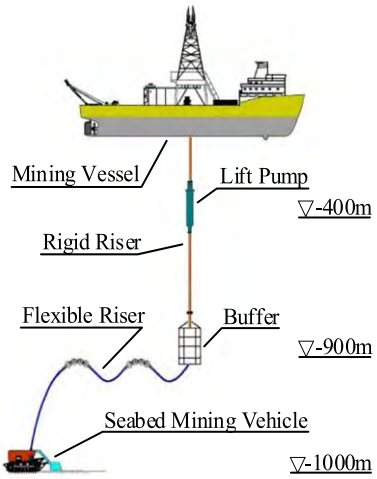

FIGURE 1. Configuration of a DSM system.

researches have been carried out for tracked vehicles on land surfaces. Mocera and Nicolini [10] proposed a multi-body model of an agricultural tracked vehicle using the program MSC.ADAMS, and pointed out that the slip and the maximum traction force would determine the final driving speed. Edwin *et al.* [11] proposed an improved single-rigid-body model of a tracked vehicle with faster computation speed and more accurate computation results compared to those of the multi-body model, and analyzed the interaction between the tracks and soft soil. Zou *et al.* [12] presented a dynamic modeling method and a motion control strategy for unmanned tracked vehicles on complex terrains based on pose and twist estimates.

The dynamic behavior of the marine riser has always been a research focus in the offshore oil exploitation field, and their researches can be consulted for investigating the seabed mining riser. Koh *et al.* [13] proposed a proper and accurate buoyancy load formulation with a high accuracy for the geometrically nonlinear analysis of a marine riser. Chen and Kim [14] studied the effects of the bidirectional inner-flow interaction dynamics on a riser based on CFD simulations, indicating that the vibration and instantaneous amplitude were mainly determined by the inner flow. Based on a large-scale model test, Wang *et al.* [15] studied the dynamic response of a water-intake riser. Cheng *et al.* [16] presented a finite element-boundary element hybrid method to investigate the nonlinear interaction between vessel waves and mooring risers, and verified the method feasibility through experiments.

To control the mining vehicle moving on the seabed sediment, Dai *et al.* [17] compared the effects of difierent path-tracking control algorithms including traditional PID, fuzzy and neural controls, and recommended the adaptive neural-fuzzy inference system control as an optimum path tracking control method. Hong *et al.* [18] designed a kinematic tracking control algorithm for an underwater mining vehicle considering the track slip and yaw, and tested the control algorithm on an experimental soil bin. Yeu *et al.* [19] adopted a vector pursuit algorithm to generate a predetermined path, presented a control algorithm for the tracked vehicle based on a relationship between the traction force and slip rate. Xia *et al.* [20] designed an adaptive estimation-based back-stepping terminal sliding controller for AUV and proved its robustness and adaptability. In addition, Purser *et al.* [21] described a type of seabed tracked vehicle that could be controlled through the Internet to investigate the effects of the ocean environment. And a dynamic controller was proposed by Bai *et al.* [22] for enhancing the path tracking accuracy based on the tire mechanics. Lima *et al.* [23] adopted the distributed nonlinear model predictive controller and estimator to enable the cooperative work of a robot team and avoid collisions with the teammates or surrounding obstacles, obtaining good control efficacy through the simulations. Premised on the fuzzy model, a general control method with better adaptation performance was applied to the heat exchanger control in [24]. Precup and Preitl [25] proposed a system development method of the input-channel non-homogeneous dynamic fuzzy controller and conducted a case study of the motor drive speed control on the basis of the sensitivity test. Vrkalovic *et al.* [26] presented a model-free synovial control method guided by the stability theory of Lyapunov. Meanwhile, the Takagi-Sugeno (T-S) fuzzy controller was designed and used in the reverse osmosis seawater desalination device control. Moreover, Yao *et al.* [27], Deng *et al.* [28], and Yao and Deng [29] introduced an adaptive robust control method using extended-state observer to control DC motor precisely, an output feedback robust controller with the backstepping design method, as well as an adaptive auto-disturbance rejection control scheme based on the full-state feedback for the motion control of hydraulic servo system respectively. A visual navigation system was developed by Wu *et al.* for the tracked vehicles and the trajectory and heading angle deviation were analyzed according to the image, where the driving motor speed was controlled by the fuzzy logic controller.

So far, however, the coordinated motion control based on a nonlinear dynamic model of the integrated DSM system still has not been achieved; consequently, the evaluation and optimization of its operation performance is yet to be finished. Owing to the high cost and extreme difficulty in carrying out the in-situ tests, the collaborative simulation is an effective way to solve the problems mentioned above. Hence, a reliable, effective nonlinear MBD model and a coordinated motion control model of the DSM system were developed in the paper.

II. DYNAMIC MODEL OF SEABED MINING VEHICLE

A. VEHICLE-SEDIMENT INTERACTION MODEL

Since the soil mechanical properties vary between the seafloor and land, a vehicle-sediment interaction model needs to be established first. In addition, the simulation program RecurDyn/Track was adopted to build the MBD model of a seabed mining vehicle, as presented in Fig. 2(b).

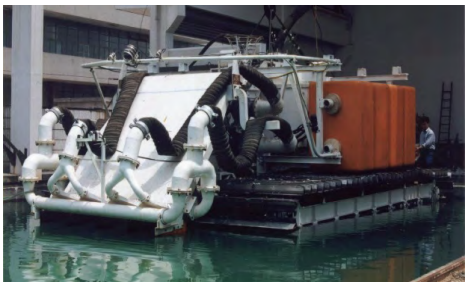

(a)

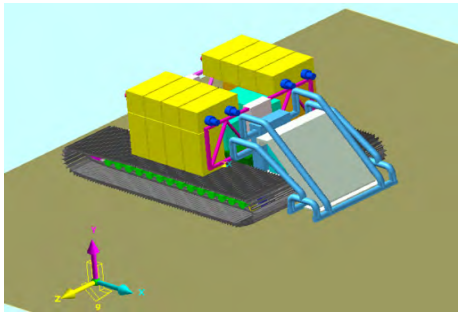

(b)

FIGURE 2. Seabed tracked mining vehicle. (a) Actual vehicle. (b) MBD model.

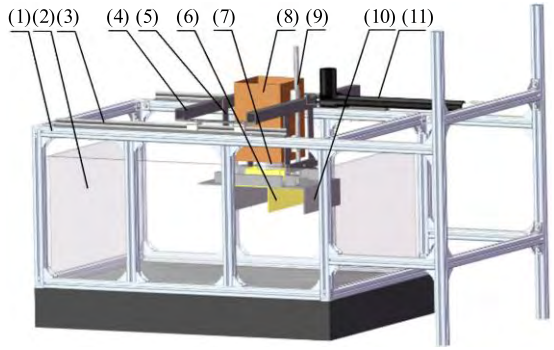

(a)

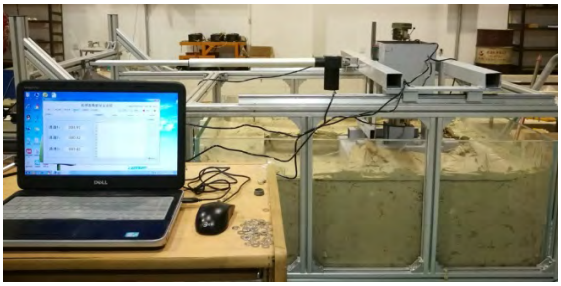

(b)

FIGURE 3. Track-sediment interaction mechanical tests. (a) Structural representation, where (1) is main frame; (2) is glass soil bin; (3) is horizontal linear guilder; (4) is lateral sliding beam; (5) is front and rear plank support; (6) is intermediate test track plate; (7) is three-axis force transducer; (8) is loading weight box; (9) is vertical guide; (10) is front and rear track plates; (11) is linear motor. (b) Actual system.

Through the laboratory imitation tests presented in Fig. 3, the normal pressure-sinkage and horizontal shear stress-displacement relationships of the track-sediment interaction were acquired.

The normal force F_{ni} acting on the ith track link element of the mining vehicle can be calculated as:

$$F_{n_i} = p_{x_i} \cdot \Delta A_i = \left[\left(\frac{k_c}{b} + k_\varphi \right) \cdot (\Delta z_i)^n \right] \cdot \Delta A_i \tag{1}$$

where p_{xi} denotes the normal pressure, A_i denotes the contact area, b denotes the track width, k_c denotes the coefficient of soil cohesive deformation, k_φ denotes the coefficient of soil friction, z_i denotes the sinkage, n denotes the soil deformability index.

The longitudinal shear force F_{longi} can be calculated as:

$$\begin{aligned} F_{long_i} = sgn\left(j_{x_i}\right) \tau_{x_i} \cdot \Delta A = sgn\left(j_{x_i}\right) \tau_{\max} \cdot K_r \cdot \Delta A \\ \cdot \left\{ 1 + \left[\frac{1}{K_r(1 - e^{-1})} - 1 \right] e^{1 - j_{x_i}/K_\omega} \right\} \\ \times \left(1 - e^{-j_{x_i}/K_\omega} \right) \end{aligned} \tag{2}$$

where j_{xi} denotes the dynamic longitudinal shear displacement, τ_{max} denotes the shear strength, K_ω denotes the shear displacement when the shear strength reaches the maximum, τ_{res} denotes the residual shear stress, and K_r is the ratio of τ_{res} to τ_{max}.

The parameter j_{xi} can be expressed as:

$$\frac{d}{dt} j_{x_i}(x_i, t) + \frac{r_s \omega_s(t)}{x_i} \cdot j_{x_i}(x_i, t) = r_s \omega_s(t) - v_x(t) \tag{3}$$

where r_s and $\omega_s(t)$ indicate the radius and angular speed of the driving wheel, x_i and $v_x(t)$ denote the distance and actual speed of the track link.

The lateral shear force F_{lati} can be expressed as:

$$\begin{aligned} F_{lat_i} = -sgn\left(j_{y_i}\right) \tau_{x_i} \cdot \Delta A = -sgn\left(j_{y_i}\right) \tau_{\max} \cdot K_r \cdot \Delta A \\ \cdot \left\{ 1 + \left[\frac{1}{K_r(1 - e^{-1})} - 1 \right] e^{1 - j_{y_i}/K_\omega} \right\} \\ \times \left(1 - e^{-j_{y_i}/K_\omega} \right) \end{aligned} \tag{4}$$

The parameter j_{yi} can be expressed as:

$$\frac{d}{dt} j_{y_i}(x_i, t) + \frac{r_s \omega_s(t)}{x_i} j_{y_i}(x_i, t) = v_{y_i}(t) \tag{5}$$

where v_{yi} denotes the lateral speed of the track link.

The vehicle-sediment interaction model was obtained by combining the above formulas. To generate a model of the deep-sea sediment, a user-defined subprogram for building the nonlinear dynamic model was developed by the C# program (refer to code at https://github.com/Walker-Yin/Model-Code.git) and integrated into the RecurDyn/Track environment.

B. CFD MODEL

Due to the non-negligible interferences acting on vehicle by the surrounding water, the analysis of the fluid resistance and resistance torque is imperative. Accordingly, a computational fluid dynamic (CFD) model of the vehicle was established, and CFD simulations for the straight-line and steering

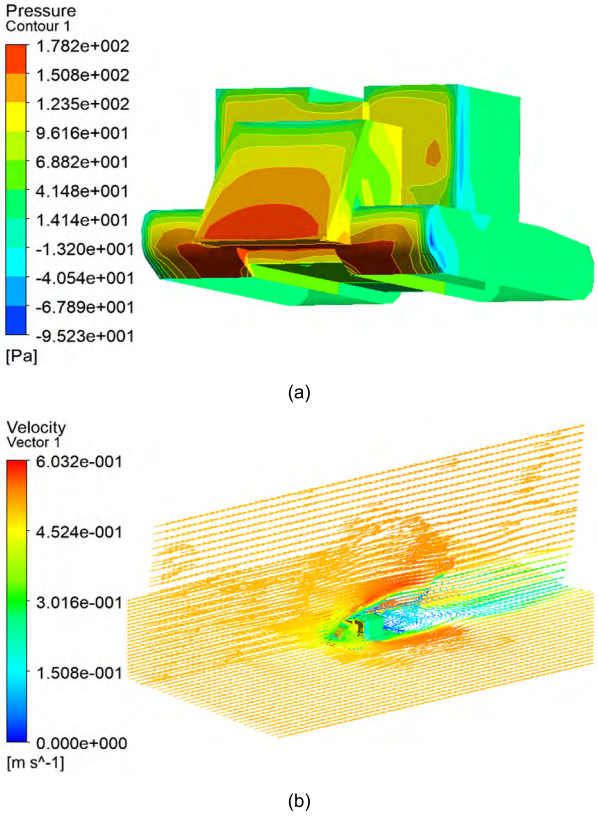

FIGURE 4. CFD simulation for straight-line motion. (a) Fluid pressure. (b) Fluid velocity.

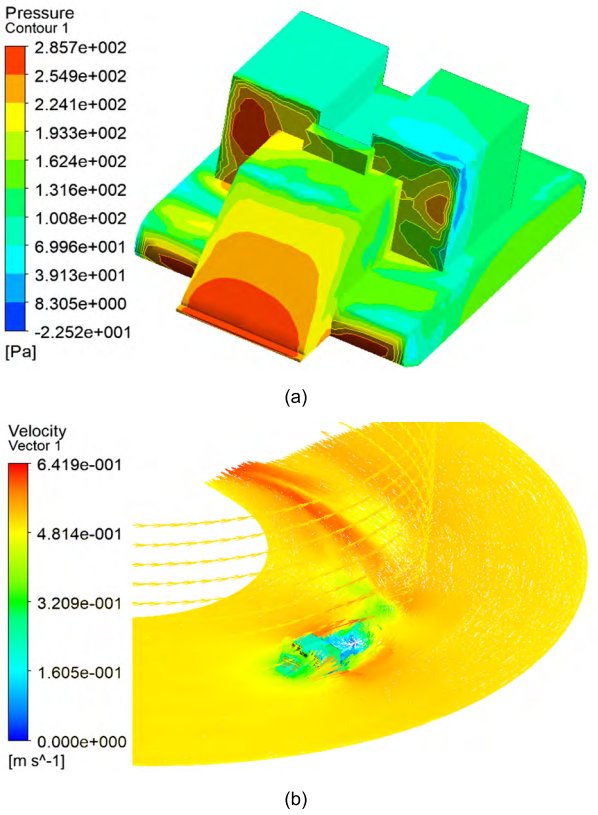

FIGURE 5. CFD simulation for turning motion. (a) Fluid pressure. (b) Fluid velocity.

motions were conducted respectively. Fig. 4 and Fig. 5 illustrate the fluid pressure and fluid velocity distributions around the vehicle.

The fluid resistance and resistance torque acting on the vehicle were obtained and loaded on five stress concentration points on the MBD model in the form of dynamic forces.

III. INTEGRATED DYNAMIC MODEL OF TOTAL SYSTEM

A. RISER MODEL

As the pipeline riser is a key component for the mineral transportation, an accurate model needs to be established to verify the performance of the riser. Compared to traditional modeling methods for risers, the discrete element method (DEM)

$$\begin{pmatrix} f_x \\ f_y \\ f_z \\ T_x \\ T_y \\ T_z \end{pmatrix} = \begin{pmatrix} \frac{2A_iE_i}{l_i} + \frac{2A_jE_j}{l_j} & 0 & 0 & 0 & 0 & 0 \\ 0 & \frac{24A_iI_{iz}}{l_i^3} + \frac{24A_jI_{jz}}{l_j^3} & 0 & 0 & 0 & \frac{8E_iI_{iz}}{l_i^2} - \frac{8E_jI_{iz}}{l_j^2} \\ 0 & 0 & \frac{24A_iI_{iy}}{l_i^3} + \frac{24A_jI_{jy}}{l_j^3} & 0 & -\frac{8E_iI_{iy}}{l_i^2} + \frac{8E_jI_{jy}}{l_j^2} & 0 \\ 0 & 0 & 0 & \frac{2J_iG_i}{l_i} + \frac{2J_jG_j}{l_j} & 0 & 0 \\ 0 & 0 & -\frac{8E_iI_{iy}}{l_i^2} + \frac{8E_jI_{jy}}{l_j^2} & 0 & \frac{2E_iI_{iy}}{l_i} + \frac{2E_jI_{jy}}{l_j} & 0 \\ 0 & \frac{8E_iI_{iz}}{l_i^2} - \frac{8E_jI_{iz}}{l_j^2} & 0 & 0 & 0 & \frac{2E_iI_{iz}}{l_i} + \frac{2E_jI_{jz}}{l_j} \end{pmatrix} \times \begin{pmatrix} x \\ y \\ z \\ \theta_x \\ \theta_y \\ \theta_z \end{pmatrix} \tag{6}$$

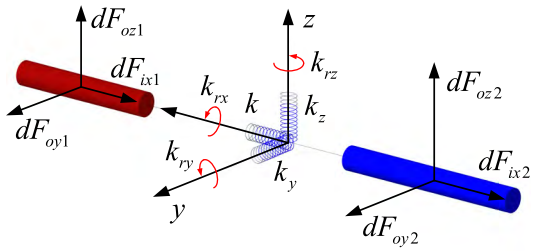

FIGURE 6. Illustration of the rigid-flexible coupled DEM model.

proves more efficient in analyzing the nonlinear dynamic behaviors for a long riser with a large displacement and rotation. The riser was built into a rigid-flexible coupled DEM model, and the external and internal fluid loads were both considered and applied to rigid elements as shown in Fig. 6.

The relative displacements, rotations, forces and torques in three-axis coordinate system between two adjacent rigid elements *i*th and *j*th in the DEM model, can be expressed as a matrix as in (6), as shown at the bottom of the previous page.

If each discrete rigid element shares the same length, the matrix (6) can be expressed as:

$$\begin{pmatrix} f_x \\ f_y \\ f_z \\ T_x \\ T_y \\ T_z \end{pmatrix} = \begin{pmatrix} \frac{AE}{l} & 0 & 0 & 0 & 0 & 0 \\ 0 & \frac{12EI_z}{l^3} & 0 & 0 & 0 & 0 \\ 0 & 0 & \frac{12EI_y}{l^3} & 0 & 0 & 0 \\ 0 & 0 & 0 & \frac{GJ}{l} & 0 & 0 \\ 0 & 0 & 0 & 0 & \frac{EI_y}{l} & 0 \\ 0 & 0 & 0 & 0 & 0 & \frac{EI_z}{l} \end{pmatrix} \times \begin{pmatrix} x \\ y \\ z \\ \theta_x \\ \theta_y \\ \theta_z \end{pmatrix} \tag{7}$$

where *x, y, z* denote the translational displacements; $\theta_x, \theta_y, \theta_z$ denote the relative rotational displacements; f_x, f_y, f_z denote the relative forces; and T_x, T_y, T_z denote the relative torques; A and l denote sectional area and length; I_y and I_z denote second moments of area; E and G denote Young modulus and shear modulus; J denotes the polar moment of inertia.

Thus, the six stiffness coefficients for the flexible connector between two adjacent rigid elements can be expressed as:

$$\begin{cases} k_x = EA/l; & k_y = 12EI_z/l^3; \ k_z = 12EI_y/l^3 \\ k_{rx} = GJ/l; & k_{ry} = EI_y/l; \ k_{rz} = EI_z/l \end{cases} \tag{8}$$

The external hydrodynamic force caused by the surface wave and sea current acting on the unit length riser can be computed as:

$$dF_o = \frac{1}{2}\rho_w C_d d_o (v_w + v_c - v_r)\,|v_w + v_c - v_r|\,dz + \frac{1}{4}\pi d_o^2 \rho_w C_m (\dot{v}_c - \dot{v}_r) dz \tag{9}$$

where ρ_w is the seawater density, C_d and C_m are the drag coefficient and the added mass coefficient, v_w and $\dot{v}_w$ are the surface wave velocity and acceleration, v_c and $\dot{v}_c$ are the current velocity and acceleration, v_r and $\dot{v}_r$ are the riser velocity and acceleration, d_o is the riser outer diameter.

The internal fluid load caused by the mixture of the mineral solid particle and seawater acting on unit length riser can be computed as:

$$dF_i = 1.06984 \times \frac{1}{2}\left(\frac{f}{d_i}\right)\rho_i v_i^2 \times \frac{1}{4}\pi d_i^2 \times dl \tag{10}$$

where f is the friction coefficient determined by the internal mixture fluid, d_i is the riser inner diameter, ρ_i is the internal mixed fluid density, v_i is the internal fluid velocity.

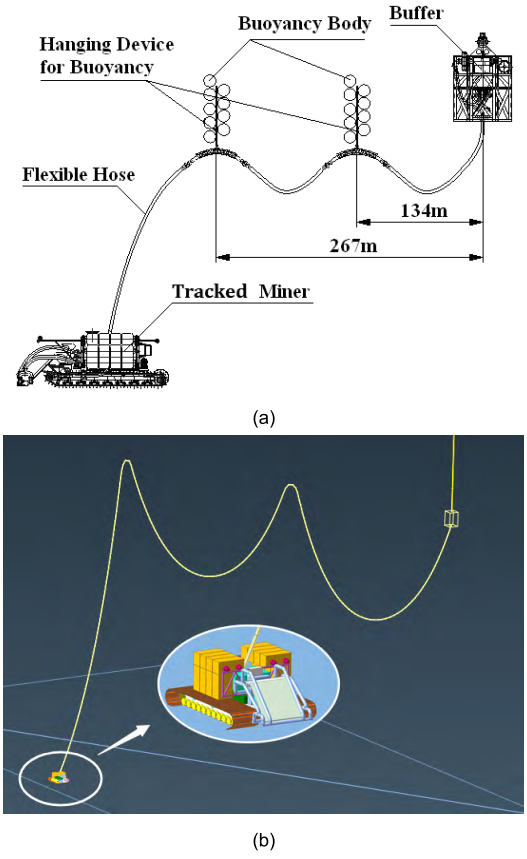

FIGURE 7. Spatial shape and buoyancy modulus of flexible riser. (a) Structural configuration. (b) Corresponding DEM simulation model.

According to the design scheme of rigid riser system, to keep its optimal spatial shape and ensure its transmission efficiency and safety, two buoyancy modules with a total buoyant force of 126 kN were installed on the flexible riser to make its spatial shape like a saddle as shown in Fig. 7.

The above DEM models of the riser, external and internal fluid loads were developed automatically by the C# program (refer to code at https://github.com/Walker-Yin/Model-Code.git) in RecurDyn/Process IDE.

B. TOTAL SYSTEM MODEL

Referring to the design parameters of China's 1000-meter sea trial system, the above models were integrated to established a nonlinear coupled MBD model of the DSM system in RecurDyn as shown in Fig. 8. Table 1 lists the main parameters of the DSM system model.

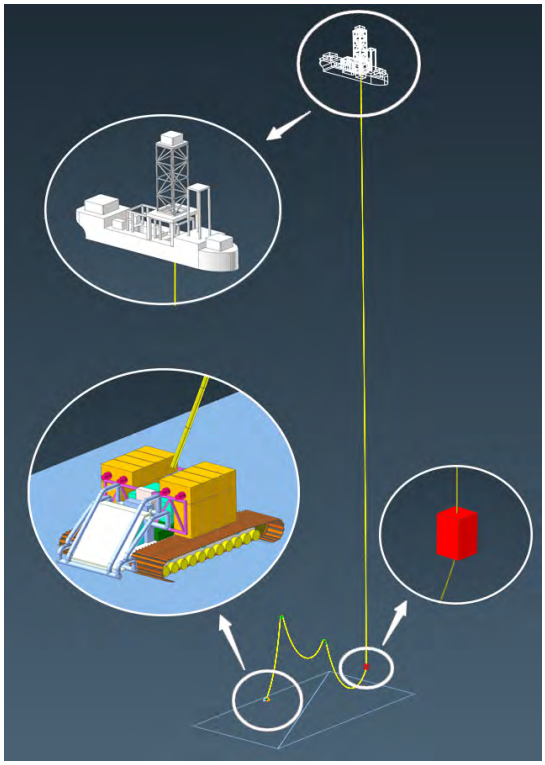

FIGURE 8. Integrated MBD model of the DSM system.

TABLE 1. Main parameters of the DSM system model.

Component	Dimension (m)		Total weight (t)	
	Length	Diameter	In air	In water
Rigid riser	900.0	0.219	75.0	46.3
Pump	6.4	0.750	7.5	6.5
Buffer	4.0 × 4.0 × 6.0		25.0	22.7
Flexible riser	300.0	0.205	12.0	7.2
Vehicle	9.3 × 5.2 × 3.0		32	11

IV. COORDINATED MOTION CONTROL MODEL

A. MATHEMATICAL MODEL FOR VEHICLE MOTION

To ensure the continuity of deep-sea mining operation process, a coordinated motion mode was recommended where the seabed vehicle moved along a predetermined mining trajectory, and meanwhile a surface mining vessel towed the riser to follow the vehicle.

In this paper, the vehicle was controlled to follow a specially-designed zigzag trajectory like a "key-hole" type illustrated in Fig. 9, to improve its sweeping coverage, collection efficiency and motion safety. A serious slip of the tracks would inevitably occur due to the weak bearing capacity and low shear strength of the seabed sediment, causing a trajectory deviation compared to its desired predetermined trajectory. Because of the condition described above, the actual trajectory deviation and heading deviation should be controlled to track its predetermined trajectory, which can be achieved by controlling the speed and speed ratio of the tracks.

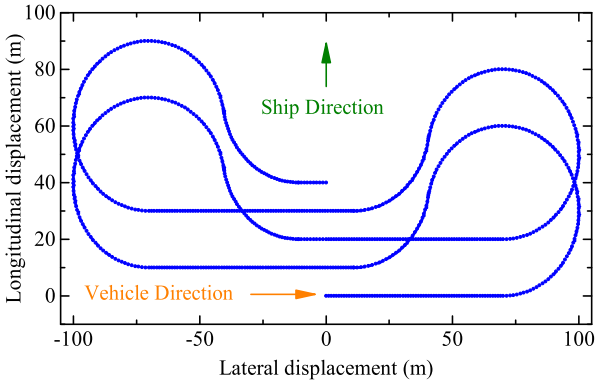

FIGURE 9. Predetermined trajectory.

The speed ratio of the left and right tracks can be expressed as:

$$i = \frac{V_r}{V_l} = \frac{V + \Delta V}{V - \Delta V} \tag{11}$$

where i is the speed ratio, V is the vehicle speed, V_r and V_l are the speeds of the right and left tracks. The vehicle moves along a straight-line when ΔV is zero.

The values V_r and V_l can be derived as follows:

$$\begin{cases} V_r = \dfrac{2i}{i+1} \cdot V \\ V_l = \dfrac{2}{i+1} \cdot V \\ \Delta V = \dfrac{i-1}{i+1} \cdot V \end{cases} \tag{12}$$

In Fig. 10, the mathematical models for the straight-line and turning motions were established. The global coordinate and vehicle-fixed coordinate systems were built. The conversion from the Cartesian coordinate to the polar coordinate in program MATLAB/Simulink can be expressed as:

$$\theta = \text{atan2}(y - y_0, x - x_0) \tag{13}$$

For the straight-line motion model:

$$\begin{cases} e = \dfrac{kx_0 + y_0 + C}{\sqrt{k^2 + 1}} \times sign(\cos\theta) \\ \alpha = \theta - \beta \\ i = 1 + \Delta i \end{cases} \tag{14}$$

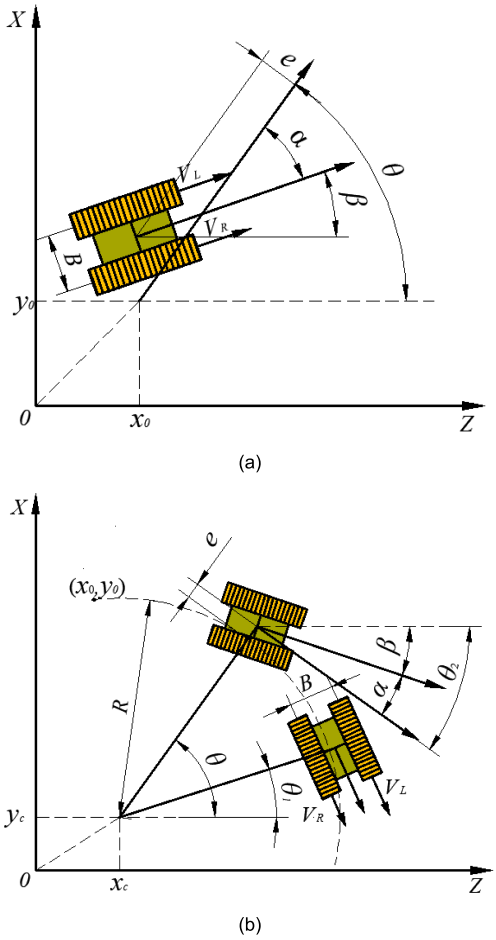

FIGURE 10. Motion models for the vehicle. (a) Straight-line. (b) Turning.

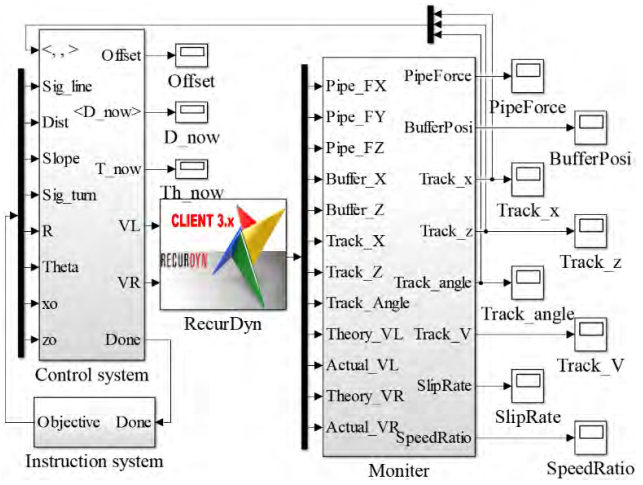

FIGURE 11. Motion control system of the vehicle.

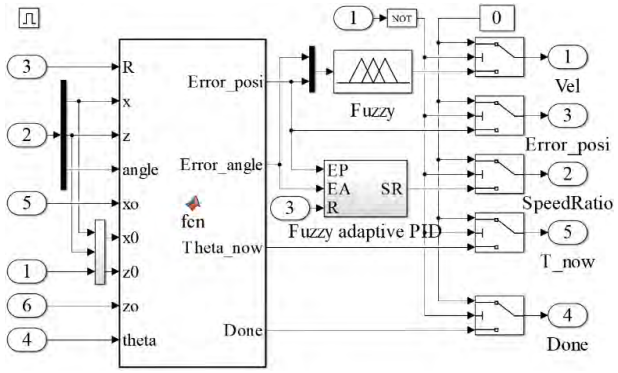

FIGURE 12. Turning motion control module.

For the turning motion model:

$$\begin{cases} e = (\sqrt{(x - x_0)^2 + (y - y_0)^2} - |R|) \times sign(R) \\ \alpha = \theta - \dfrac{\pi}{2} \times sign(R) - \beta \\ \Delta\theta = \theta - \theta_1 \\ i = \dfrac{R + B/2}{R - B/2} + \Delta i \end{cases} \tag{15}$$

where (x_0, y_0) denotes the initial coordinate, (x_c, y_c) denotes the turning center coordinate, β denotes the actual heading angle, θ denotes the heading angle of predetermined trajectory, $e$denotes the trajectory deviation, α denotes the heading deviation, B denotes the distance between the centerlines of two tracks.

B. MOTION CONTROL MODEL

In Fig. 11, a collaborative simulation model was established according to the above mathematical models, in which the vehicle was controlled to track a predetermined trajectory combined by straight line trajectories and turning circular arc trajectories. An integrated motion control system and a total dynamic model were built in MATLAB/Simulink and RecurDyn respectively. In the motion control system, a monitoring module can read, convert and store the dynamic parameters from the RecurDyn model; a control module can calculate the trajectory deviation, heading deviation, slip and speed ratio, and output the desired speed of left and right tracks of the vehicle.

Fig. 12 shows the turning motion control module. Firstly, it can calculate the trajectory deviation (e), heading deviation (α), and turning angle ($\Delta\theta$); then, proper speed and speed ratio are obtained by the fuzzy control algorithm and fuzzy adaptive PID control algorithm; finally, the speed of left and right tracks are calculated by formula (14) and input into the dynamic model in RecurDyn.

Due to the influences of the vehicle-sediment interaction, fluid resistance and other factors, the system possesses highly complex nonlinear characteristics, leading to the difficulty in establishing an accurate model. Hence, a fuzzy adaptive PID control algorithm with a good adaptability to the nonlinear and model system unknown was adopted to control the speed ratio increment (Δi), where the trajectory deviation and heading deviation were the input variables. Moreover, the fuzzy adaptive PID control module was developed by toolbox in MATLAB/Simulink with the gain of 0.6.

Fig. 13 illustrates the fuzzy adaptive PID control algorithm built for controlling the turning speed ratio, taking the trajectory deviation and heading deviation as input variables.

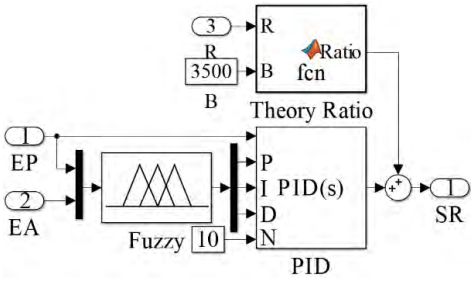

FIGURE 13. Fuzzy adaptive PID control algorithm.

TABLE 2. Fuzzy control rules.

Velocity		Heading deviation (α)						
		NB	NM	NS	ZO	PS	PM	PB
Trajectory deviation (e)	NB	NB	NB	NS	ZO	PS	PM	PM
	NM	NM	NS	ZO	PS	PM	PB	PM
	NS	NS	ZO	PS	PM	PB	PM	PS
	ZO	ZO	PS	PM	PB	PM	PS	ZO
	PS	PS	PM	PB	PM	PS	ZO	NS
	PM	PM	PB	PM	PS	ZO	NS	NM
	PB	PM	PM	PS	ZO	NS	NB	NB

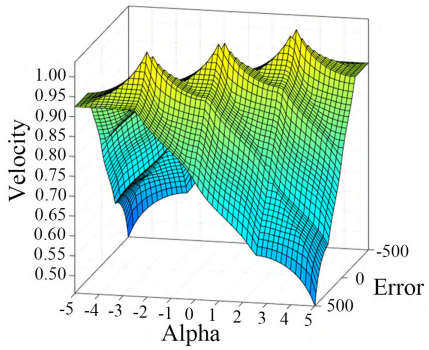

FIGURE 14. Fuzzy control output domain.

The fuzzy control rules were listed in Table 2 and the output domain of speed obtained by the rules was displayed in Fig. 14.

V. CO-SIMULATION RESULTS AND DISCUSSION

The data exchange between RecurDyn and Simulink was established, with the co-simulation carried out, and then the data recorded by the motion control system was discussed.

Fig. 15 illustrates the actual tracking trajectory and its deviation compared to the predetermined trajectory. As presented, the trajectory deviation could be generally controlled within 0.5 m during the 1100-second motion process. Because of a relatively severe slip of the tracks, the maximum deviation reached approximately 0.7 m. Specifically, the trajectory deviation increased and then decreased when switches occurred between the straight line and the arc trajectories. The overall process can satisfy the requirement of the path tracking accuracy within 1 m for the vehicle.

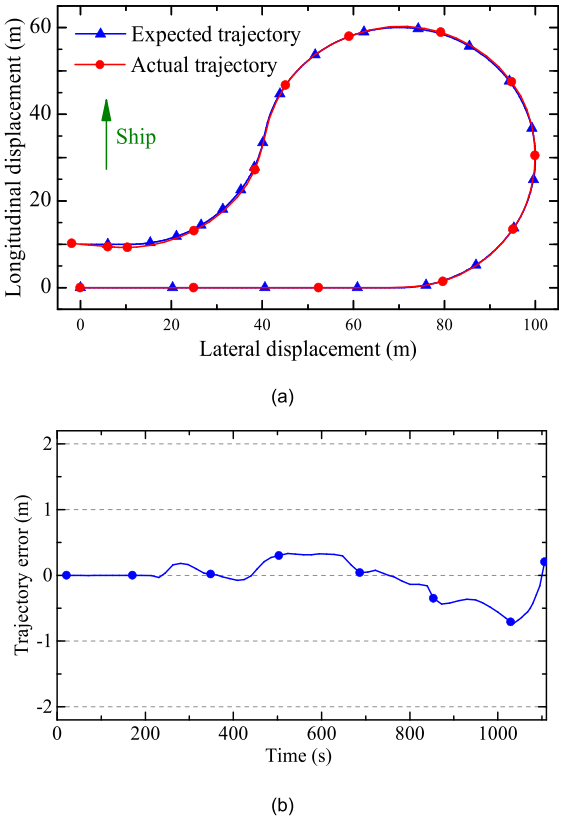

FIGURE 15. Trajectory tracking for the vehicle. (a) Actual and predetermined trajectories. (b) Trajectory deviation.

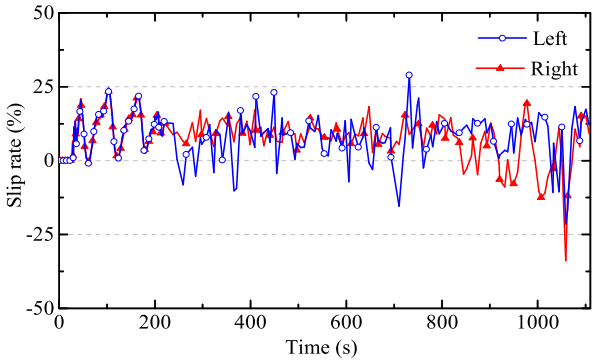

FIGURE 16. Slip rates of the tracks.

Furthermore, compared with the turning motion, the trajectory tracking during straight-line motion was more accurate.

It is generally recognized that a greater slip for the vehicle will occur on account of the low bearing capacity and weak shear strength of the sediment. Fig. 16 shows the slip of both tracks which generally fluctuates within 25%, with an average slip of approximately 10%, proving that the vehicle possesses an acceptable motion stability.

The motion stability and continuity for the mining riser during the continuous operation were particularly crucial to ensure the transportation safety and efficiency for the mineral particles. As shown in Fig. 17, the spatial trajectories of the buffer and the buoyancy modules were smooth, without

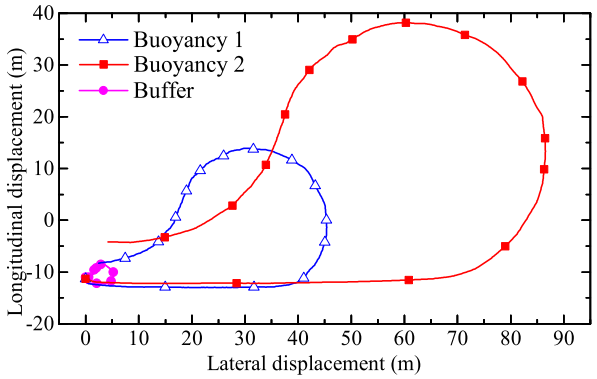

FIGURE 17. Trajectories of the buffer and buoyancy bodies.

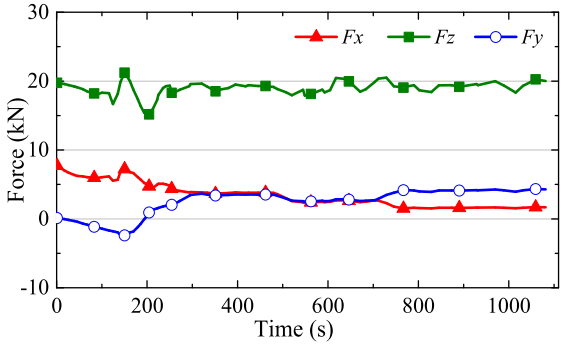

FIGURE 18. Three-direction forces acting on the vehicle by the flexible riser.

the serious swings, twines or overstretches. Additionally, the buffer motion range was small and its maximum swing reached no more than 10 m. Consequently, the maximum deflection angle of the rigid riser would not exceed 2 degrees, which is a safe operation range.

Fig. 18 presented the three-direction forces acting on the mining vehicle caused by the flexible riser and F_x, F_y, F_z represented the forces along the longitudinal, lateral and vertical directions, respectively. The vertical force fluctuated around 20 kN; the initial longitudinal force stood at about 7.5 kN, and it would decrease and maintain at about 2 kN; there was no lateral force initially, however, with the coordinated motion, it would increase and maintain at about 5 kN.

VI. CONCLUSIONS

The main conclusions reached from this investigation include the following:

1) A nonlinear interaction model between a seabed mining vehicle and the sediment was derived. The fluid resistance and resistance torque acting on the vehicle were obtained by CFD numerical simulations and applied to the MBD model. A Subprogram for building a nonlinear DEM model of the long mining riser was developed by C# programs. Based on these, a nonlinear MBD model of a DSM system was established.
2) A motion control system for predetermined path tracking of the seabed mining vehicle was developed in which the fuzzy control algorithm and fuzzy adaptive PID control algorithm were adopted to control the speed and speed ratio of the tracks respectively.
3) The coordinated motion simulation for the DSM system was achieved based on the co-simulation between the control model and the dynamic model. It demonstrated that the trajectory tracking accuracy for the mining vehicle could be controlled effectively to meet the requirement, and the DSM system could keep a stable motion state during the continuous operation process.
4) The future work will prioritize the development of vehicle motion control system, the adoption of various algorithms and multiple control variables to further improve the path tracking accuracy, vehicle stability and slip control in real time.

REFERENCES

[1] J. S. Chung, "Deep ocean mining technology III: Developments," presented at the 8th ISOPE Ocean Mining Symp., Chennai, India, Sep. 2009.
[2] Y. Dai, X. Zhu, L. S. Chen, H. Liu, T. Zhang, and S. J. Liu, "A new multi-body dynamic model for seafloor miner and its trafficability evaluation," *Int. J. Simul. Model.*, vol. 14, no. 4, pp. 732–743, 2015.
[3] Y. Dai, X. Zhu, and L. S. Chen, "A mechanical-hydraulic virtual prototype co-simulation model for a seabed remotely operated vehicle," *Int. J. Simul. Model.*, vol. 15, no. 3, pp. 532–541, 2016.
[4] Y. Dai, L. S. Chen, X. Zhu, and H. Liu, "Modelling and simulation of a mining machine excavating seabed massive sulfide deposits," *Int. J. Simul. Model.*, vol. 15, no. 2, pp. 377–387, 2016.
[5] L. Li and J. Zhong, "Research of China's pilot-miner in the mining system of poly-metallic nodule," presented at the 6th ISOPE Ocean Mining Symp., Changsha, China, Oct. 2005.
[6] F. Xu, Q.-H. Rao, and W.-B. Ma, "Turning traction force of tracked mining vehicle based on rheological property of deep-sea sediment," *Trans. Nonferrous Met. Soc. China*, vol. 28, pp. 1233–1240, Jun. 2018.
[7] S. Umaru, S.-J. Liu, and Q.-J. Han, "Modeling of miner track system during steering motion," *J. Central South Univ.*, vol. 22, no. 2, pp. 502–510, 2015.
[8] M. T. Vu, H.-S. Choi, J.-Y. Kim, and N. H. Tran, "A study on an underwater tracked vehicle with a ladder trencher," *Ocean Eng.*, vol. 127, pp. 90–102, Nov. 2016.
[9] S.-H. Baek, G.-B. Shin, and C.-K. Chung, "Experimental study on the soil thrust of underwater tracked vehicles moving on the clay seafloor," *Appl. Ocean Res.*, vol. 86, pp. 117–127, May 2019.
[10] F. Mocera and A. Nicolini, "Multibody simulation of a small size farming tracked vehicle," *Procedia Struct. Integr.*, vol. 8, pp. 118–125, Jan. 2018.
[11] P. Edwin, K. Shankar, and K. Kannan, "Soft soil track interaction modeling in single rigid body tracked vehicle models," *J. Terramechan.*, vol. 77, pp. 1–14, Jun. 2018.
[12] T. Zou, J. Angeles, and F. Hassani, "Dynamic modeling and trajectory tracking control of unmanned tracked vehicles," *Robot. Auton. Syst.*, vol. 110, pp. 102–111, Dec. 2018.
[13] K. J. Koh, A. Y. M. Yassin, and M. Latheef, "On the buoyancy load formulation for geometrically nonlinear analysis of flexible marine risers," *Ocean Eng.*, vol. 157, pp. 313–324, Jun. 2018.
[14] Z.-S. Chen and W.-J. Kim, "Effect of bidirectional internal flow on fluid–structure interaction dynamics of conveying marine riser model subject to shear current," *Int. J. Nav. Archit. Ocean Eng.*, vol. 4, pp. 57–70, Mar. 2012.
[15] J. Wang, S. Xiang, S. Fu, P. Cao, J. Yang, and J. He, "Experimental investigation on the dynamic responses of a free-hanging water intake riser under vessel motion," *Mar. Struct.*, vol. 50, pp. 1–19, Nov. 2016.
[16] Y. Cheng, C. Ji, G. Zhai, and G. Oleg, "Nonlinear analysis for ship-generated waves interaction with mooring line/riser systems," *Mar. Struct.*, vol. 59, pp. 1–24, May 2018.

[17] Y. Dai, X. Zhu, H. Zhou, Z. Mao, and W. Wu, "Trajectory tracking control for seafloor tracked vehicle by adaptive neural-fuzzy inference system algorithm," *Int. J. Comput. Commun. Control*, vol. 13, no. 4, pp. 465–476, 2018.
[18] S. Hong, J.-S. Choi, H.-W. Kim, M.-C. Won, S.-C. Shin, J.-S. Rhee, and H.-U. Park, "A path tracking control algorithm for underwater mining vehicles," *J. Mech. Sci. Technol.*, vol. 23, no. 8, pp. 2030–2037, 2009.
[19] T.-K. Yeu, S.-J. Park, S. Hong, H.-W. Kim, and J. S. Choi, "Path tracking using vector pursuit algorithm for tracked vehicles driving on the soft cohesive soil," presented at the SICE-ICASE Int. Joint Conf., Busan, South Korea, Oct. 2006.
[20] Y. Xia, K. Xu, Y. Li, G. Xu, and X. Xiang, "Adaptive trajectory tracking control of a cable-driven underwater vehicle on a tension leg platform," *IEEE Access*, vol. 7, pp. 35512–35531, 2019.
[21] A. Purser, L. Thomsen, C. Barnes, M. Best, R. Chapman, M. Hofbauer, M. Menzel, and H. Wagner, "Temporal and spatial benthic data collection via an Internet operated deep sea Crawler," *Methods Oceanogr.*, vol. 5, pp. 1–18, Apr. 2013.
[22] G. Bai, L. Liu, Y. Meng, W. Luo, Q. Gu, and J. Wang, "Path tracking of wheeled mobile robots based on dynamic prediction model," *IEEE Access*, vol. 7, pp. 39690–39701, 2019.
[23] P. U. Lima, A. Ahmad, A. Dias, A. G. S. Conceição, A. P. Moreira, E. Silva, L. Almeida, L. Oliveira, and T. P. Nascimento, "Formation control driven by cooperative object tracking," *Robot. Auton. Syst.*, vol. 63, no. 1, pp. 68–79, 2015.
[24] I. Škrjanc, S. Blažič, and D. Matko, "Model-reference fuzzy adaptive control as a framework for nonlinear system control," *J. Intell. Robot. Syst.*, vol. 36, no. 3, pp. 331–347, 2003.
[25] R.-E. Precup and S. Preitl, "Development of fuzzy controllers with non-homogeneous dynamics for integral-type plants," *Elect. Eng.*, vol. 85, no. 3, pp. 155–168, 2003.
[26] S. Vrkalovic, E.-C. Lunca, and I.-D. Borlea, "Model-free sliding mode and fuzzy controllers for reverse osmosis desalination plants," *Int. J. Artif. Intell.*, vol. 16, no. 2, pp. 208–222, 2018.
[27] J. Yao, Z. Jiao, and D. Ma, "Adaptive robust control of DC motors with extended state observer," *IEEE Trans. Ind. Electron.*, vol. 61, no. 7, pp. 3630–3637, Jul. 2014.
[28] W. Deng, J. Yao, and D. Wei, "Time-varying input delay compensation for nonlinear systems with additive disturbance: An output feedback approach," *Int. J. Robust Nonlinear Control*, vol. 28, no. 1, pp. 31–52, Jan. 2018.
[29] J. Yao and W. Deng, "Active disturbance rejection adaptive control of hydraulic servo systems," *IEEE Trans. Ind. Electron.*, vol. 64, no. 10, pp. 8023–8032, Oct. 2017.
[30] X. Wu, Y. Zhang, T. Zou, L. Zhao, P. Lou, and Z. Yin, "Coordinated path tracking of two vision-guided tractors for heavy-duty robotic vehicles," *Robot. Comput. Integr. Manuf.*, vol. 53, pp. 93–107, Oct. 2018.

YU DAI was born in Hunan, China, in 1981. He received the B.S., M.S., and Ph.D. degrees from the College of Mechanical and Electrical Engineering, Central South University (CSU), Changsha, China, in 2003, 2006, and 2010, respectively. He finished the Postdoctoral research in control theory and engineering at CSU, in 2013.

He is currently an Associate Professor and the Deputy Director of the Mechatronics Department, College of Mechanical and Electrical Engineering, CSU. He has been a Visiting Scholar at Shanghai Jiao Tong University and now the joint researches are being conducted. He is also the Project Evaluation Expert for the National Natural Science Foundation of China. He has presided over 20 national, ministerial, and provincial scientific research projects. His major research interests include the design and control of complex electro-mechanical systems, vehicle dynamics and control, rotorcraft's transmission, and lubrication system design and simulation.

Dr. Dai is a Senior Member of the Chinese Mechanical Engineering Society. He received the Reward-Gainer of the Excellent Doctor Degree Dissertation.

WANWU YIN was born in Hunan, China, in 1994. He received the B.S. degree in mechanical and electrical engineering from the Central South University of Forestry and Technology, Changsha, China, in 2017. He is currently pursuing the M.S. degree in mechanical and electrical engineering with Central South University.

He is conducting research on pipeline modeling, miner environment loads' analysis, and motion control system design of the deep-sea mining systems and its dynamic simulation under the guidance of Prof. Y. Dai.

FEIYUE MA was born in Anhui, China, in 1993. He received the B.S. degree in mechanical engineering from the Central South University of Forestry and Technology, Changsha, China, in 2017. He is currently pursuing the M.S. degree in mechanical engineering with the College of Mechanical and Electrical Engineering, Central South University, Changsha.

His research interests include computational fluid dynamics, oil jet lubrication, nozzle optimization design, and windage power loss of the aeronautical transmission systems.